I. P. N. - 91406 ORSAY CEDEX

institut de physique nucléaire CNRS - IN2P3 UNIVERSITE PARIS - SUD

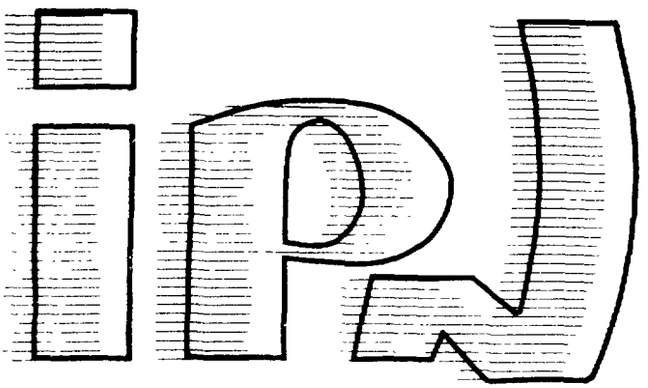

ION DESORPTION PHENOMENA INDUCED BY VARIOUS TYPES OF MULTIPLY CHARGED PROJECTILES AND BY PHOTONS ON SOLID SURFACES

Y. LE BEYEC

Lectures given at the "Escola Latino Americana de Fisica, ELAF91", CAXAMBU, BRASIL, August 1991.

Ion desorption phenomena are the general denomination for the emission of ions (atomic, molecular, clusters) from solid samples - generally insulating organic or inorganic materials - bombarded by accelerated ions or electrons, or by photons (laser).

The understanding of the desorption mechanisms is to day an attractive problem of fundamental physics linked to energy deposit and transfer in solids. The great potential of the desorption processes, to investigate interactions between fast ions and materials and to develop analytical tools, explains the increasing number of scientists and laboratories devoting their interest to ion desorption.

New experiments require the construction of specific equipments and the use of advanced technologies but, with the exception of beams from accelerator, relatively simple and light experimental facilities are necessary. The wide range of options to study ion desorption and the large number of possible applications - that has demonstrated the interdisciplinarity of the field - make the all domain, a good choice, for emerging research groups.

It is a great pleasure to participate into the "Escola Latino Americana de Fisica, ELAF91" and to have the opportunity to talk on this subject. I have summarized, in the following, some of the work done in our laboratory during the past recent years. I have tried to show, by various types of experiments and results that this field of research is a source of fruitful developments. I did not cover, neither the applications that would have required a rather long paragraph, nor the instrumental part which is, of course, also very important. The I.P.N. (Institut de Physique Nucléaire Orsay) is known for its contribution to many other laboratories and colleagues.

I believe in the rapid growing of the field - including companies involved in instrumentation - and, in the future of massive ion impacts. All domains of applications will gain from fundamental experiments.

Orsay, May 1991

ION DESORPTION PHENOMENA INDUCED BY VARIOUS TYPES OF MULTIPLY CHARGED PROJECTILES AND BY PHOTONS ON SOLID SURFACES

Y. LE BEYEC

Institut de Physique Nucléaire, 91406 - Orsay Cedex, France

The field of desorption-ionization of secondary species induced by fast and slow ions in a solid is extremely large (fast and slow will be defined later). A collision betweeen a two atom system or more generally a two-body system is relatively simple to describe even if the interacting potentials are not completely known. When a large number of atoms and complex ions are involved in multiple collisions, understanding the detailed processes that occur in a short time after the initial interaction is an ambitious goal. The complex sequence of dynamical events in the solid that finally lead for example, to the ejection into the gas phase of intact molecules is poorly understood. In recent years however a certain number of efforts in several laboratories have contributed to elucidate the basic phenomena. A large variety of applications has been developed and has demonstrated the interdisciplinarity of the field. Until now mainly single atoms or ions (sometimes multiply charged ions) were used to interact with solid materials. More recently, cluster ions have been used as projectiles. Small power density lasers have also been used recently to eject intact molecular ions from the surface.

In all cases, whatever the initial triggering process, the energy that is deposited in the solid must be coupled to atomic and molecular motion.

In these lectures, I will summarize some of the results obtained in experiments performed at our laboratory, Institut de Physique Nucléaire Orsay, France (Ion-Surface and Material Interactions Group). In these experiments we have used several types of projectiles at various energies.

I. GENERAL REMARKS

For simplification it is generally considered that there are two regimes of primary ion velocities that correspond to two distinct classes of mechanisms of interaction. The "critical" value of velocity that "separates" the two regimes is the Bohr velocity $V_0 = \frac{e^2}{\hbar}$. When the velocity of the primary ion (PI) V_p is small, target electrons move much faster than the projectile and the primary ions interact with the whole atoms. Atomic collisions take place. When the velocity of the PI is large compared to the electron velocity in the

target atoms ($V_p \gg V_0$), the PI "sees the electrons at rest", and there are interactions with electrons. In this case, electronic collisions occur. There is of course an overlapping region of primary ion velocities where the two processes are both present.

In the following, experiments will be described in the two regimes of velocity. V_0 is about 0.2 cm/nsec and corresponds to an energy per mass unit of 25 keV/u ($E_{MeV/u} = \frac{1}{2} V^2$ with V in cm/nsec). The quantity E/u is a practical unit that will be employed in the next sections.

Energy loss mechanisms are therefore related to the two regimes of velocities and correspond to the so-called nuclear stopping power ($V_{PI} < V_0$) and electronic stopping power ($V_{PI} > V_0$). The nuclear stopping power is based on elastic two particle collisions between M_1 and M_2, with M_2 at rest. $E_{M_1 i}$ is the initial energy, $E_{M_1 f}$ is the final energy of M_1 after having transferred an energy E_2 to M_2. φ_1 and φ_2 are the scattering and recoil angle in the laboratory system. θ is the center of mass scattering angle and E_{CM} the energy in the center of mass system. Classical conservation laws lead to the following basic formulas :

$$E_{recoil} = E_2 = E_{M_1 i} - E_{M_1 f}$$

$$E_{CM} = \frac{4\, M_1\, M_2}{(M_1 + M_2)^2} \times E_{M_1 i} \quad \text{and} \quad E_{recoil} = E_{CM}.\sin^2 \theta/2$$

with $$\theta = \pi - 2p \int_{R_{min}}^{\infty} \frac{d\, R/R^2}{\sqrt{1 - V_{(R)}/E_R - P^2/R^2}}$$

where R is the distance between two nuclei, R_{min} the minimum distance of approach, $V_{(R)}$ the interatomic potential and p the impact parameter. Different values can be assumed for $V_{(R)}$. The nuclear stropping power dE/dx can be approximated through most of the keV energy regions as [1] :

$$\frac{dE}{dx} \simeq 1.3\, \pi\, Na\, Z_1 Z_2\, e^2\, \frac{M_1}{M_1 + M_2}$$

where N is the target atomic density (atoms/cm^3), Z_1, Z_2 atomic numbers, a is a numerical constant $\simeq 0.5\, (Z_1^{2/3} + Z_2^{2/3})^{-1/2}$.

Simple expressions have also been derived by W.Wilson et al [3] for the nuclear stopping :

$$\frac{dE}{dx} = S_n(\varepsilon) \cdot \pi a^2 \gamma N \cdot \frac{\varepsilon}{E}$$

with $\varepsilon = \dfrac{aM_2E}{Z_1Z_2e^2(M_1+M_2)}$ $\gamma = \dfrac{4M_1M_2}{(M+M_2)^2}$

and $S_n = \dfrac{0.5 \ln(1+\varepsilon)}{\varepsilon - A\varepsilon^B}$ $A = 0.1412$ and $B = 0.42059$

Multiple scattering, path length distributions, displacement damages, and three dimensional evaluation make a complete calculation very complex. A very convenient P.C. program is now available : "TRIM" [3] that allows calculation of most of the needed simulations with a variety of projectiles and targets. Standard sputtering theory is used. An example of calculation is given in Fig. 1.

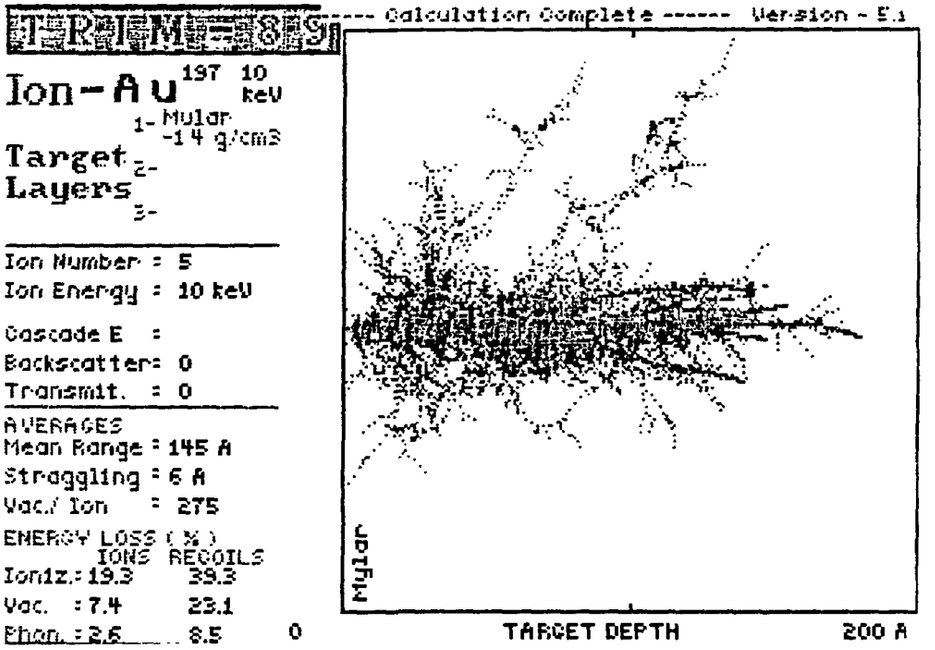

Figure 1 : Example of output with the program TRIM.

At large velocity the energy loss is based on collisions between a primary ion with charge Z_1 at velocity V and an electron "at rest" at a distance b from the PI trajectory. The maximum acting force is Z_1e^2/b^2 with an estimated time of collision of 2b/V. The transferred momentum is roughly equal to $\Delta p \simeq \dfrac{2Z_1e^2}{bV}$ and the energy absorbed in the collision $\delta E \simeq \dfrac{\Delta p^2}{2M} = \dfrac{2Z_1e^4}{MV^2b^2}$. If

electrons in a solid have a volumetric density of n_0 , then the energy loss in a thickness dx at a distance b from the PI ion path is $dE = \delta E \times 2\pi bdb.dx.n_0$. Between minimum distances b_{min} and b_{max} we have :

$$\frac{dE}{dx} = \frac{4\pi Z_1{}^2 e^4 n_0}{MV^2} \int_{b_{min}}^{b_{max}} \frac{db}{b}$$

b_{max} and b_{min} can be approximated according to the PI velocities [4]. An approximated expression, for a projectile with charge Z_1 and an atom with Z_2 electrons, is given by the Bethe formula [5] :

$$\frac{dE}{dx} = \frac{4\pi Z_1{}^2 e^4 n_0 Z_2}{MV^2} \left\{ \log \frac{2MV^2}{I} \right\}$$

Empirically, I is the mean ionization energy and $I \simeq 10\ Z_2$ (eV) for $Z_2 \gg 1$. Z_2 is the target atomic number.

More complete formulas can be derived from a more detailed description of the energy loss. In any case, theoretical values have to be adapted to experimental values, and for practical purposes, adjustable parameters have been introduced into the formula's derivation.

The charge $q_1 = Z_1$ of the primary ion is a very critical parameter since this parameter changes rapidly when the primary ion penetrates in a solid. There is even a charge distribution probability according to the cross sections of gain or loss of electrons by a fast ion traveling through the material. Electronic stopping power values have been tabulated by several authors [6-8]. Frequently, there are large discrepancies between these values. In addition, comparisons between calculated and experimental values show differences that can reach 30 to 40 %. Experiments are clearly needed to obtain reliable values.

Our goal is not to develop here energy loss theories but to emphasize the distinction between the two modes of energy loss. We are interested in the final step, that follows the energy loss and transfer mechanisms, i.e. the emission of secondary species from the surface.

Atomic collision cascades and the sputtering theory can reproduce the emission of atoms relatively well, but as already mentioned, the simultaneous emission of an assembly of atoms (as a molecule) is more difficult to explain.

II. ENERGETIC PROJECTILES : MEV IONS AND MOLECULAR ION EMISSION

In the first part I will discuss results with fast ions above 0.2 MeV/u. When a solid material is bombarded by such energetic particles, molecular ions ion-clusters and neutrals are ejected from the surface[1]. The yield of emission, which can be very important, ranges from 0.1 to 10^5 per impact depending on the material, the amount of energy loss, the type of surface,etc.

We will distinguish the entrance channel and the exit channel in the interaction. In the entrance channel we have several parameters :

- the type of ions, the velocity, the charge state (and equilibrium charge state),
- the angle of incidence with the surface,
- the nature of the surface and material.

In the exit channel we may consider :

- the type of secondary ions, i.e. atomic, molecular ions, cluster ions...
- the type of neutrals,
- the secondary ion yield, i.e. the number of SI per primary ions,
- the secondary electron yield,
- the energy and angular distribution of the emitted species,
- the stability of the molecular ions.

The phenomena observed in the exit channel correspond to the solid's response to the interaction. They depend on the parameters in the entrance channel. Therefore, a study of the variation of these parameters gives some insight into the mechanisms.

II.1. Experimental method

Heavy ion beams from accelerators were used with energies per mass unit between 0.3 and 5 MeV. Ions of ^{32}S to ^{235}U have been delivered by a cyclotron, a Tandem machine in Orsay and a linear accelerator in Darmstadt. Experiments have also been performed at Uppsala, Erlangen, Argonne, Catania. I suggest that the readers look at ref. [9-14] for more information. Briefly, a beam of heavy ions is selected in mass and energy by the accelerator before entering a reaction chamber where targets are positioned in the center. Variation of the

~~~~~~~~~~~~~~~~

[1]Prof. R. Macfarlane from Texas A&M has initiated this field. A special issue of "Int. J. of Mass Spectrometry and Ions Processes" has been dedicated to R. Macfarlane, vol. 53 (1983).
~~~~~~~~~~~~~~~~

energy is achieved either by changing the machine parameters or by inserting metallic absorber foils in the beam prior to the target. For experiments with a specific charge state, the beam passes first through a thin foil of carbon (10 μ) or gold (10 μ) to produce a distribution of charge states. The charge state desired is selected by a magnet, and the resulting low intensity ion beam (100 to 500 ions/sec) is collimated to 1 mm diameter before striking the target. Fig. 2 shows a schematic diagram of the experimental geometry. The energy of the primary ion is monitored and controlled by a Si detector after passing through the target. A vacuum of 10^{-7} torr is maintained in the system by a cryopump. These are counting experiments, and for each ion hitting the target, the secondary ions emitted from the target surface are identified and counted. Secondary ion yields are measured according to the entrance channel parameters.

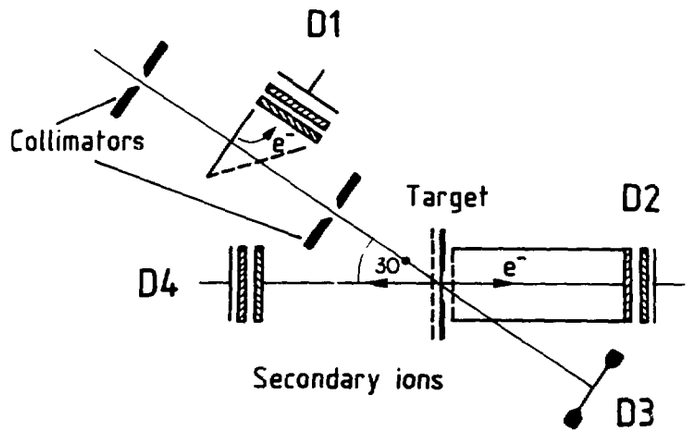

Figure 2
Experimental arrangement for on beam experiments
- *D1, D2, D4 are micro-channel plate detectors for time signals*
- *D3 is a silicon detector for energy signals and time signals*

Time of flight (TOF) mass spectrometry is used to identify secondary ions. This technique is a very simple and efficient technique. Several developments and pieces of semi-commercial equipment have been made at the Institut ; e.g. fast electronics, time digital converters and data acquisition systems. TOF mass spectrometers for analytical applications have even been built. More details on the techniques and the electronics can be obtained from ref. [15-17].

In experiments with accelerator-beams, time of flight distances shorter than 20 cm were generally used for secondary ions and secondary electrons as well.

Targets consist of thin films of materials deposited on metallic backing by evaporation under vacuum or by electrospray. Different types of sample compounds have been used (inorganic and organic).

II.2. P.I. velocity dependence

The SI yield as well as the total sputtering yield depend on the PI velocity. The velocity dependence has been observed in many cases with targets of condensed gases, H_2O films [18-20], inorganic films, and organic films [21-23,11,13]. An example, already shown in ref. [24], is presented below in Fig. 3. A rapid increase of the SI yield is observed above 0.4 cm/nsec followed by a maximum at about 1-1.2 cm/nsec. Similar trends have been obser-

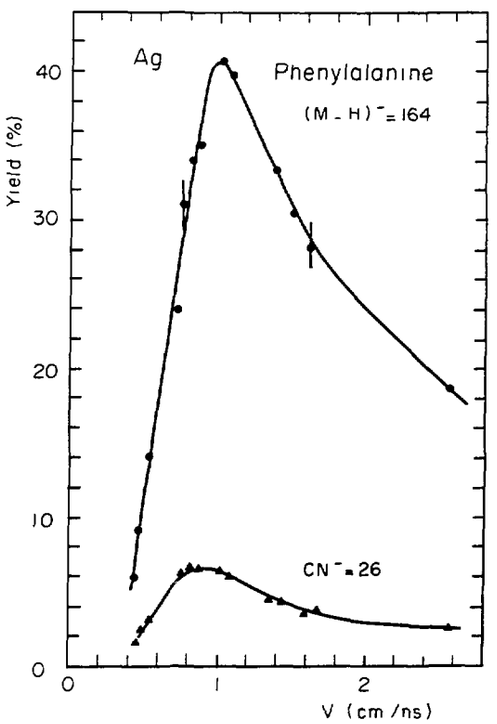

Figure 3
Variation of the desorption yield of molecular ion $(M-H)^-$ from a phenylalanine sample as function of velocity of Ag ions.

ved for several compounds. The parameter "velocity" is not a simple parameter because the primary ion charge state varies with the PI velocity. As seen before, dE/dx is proportional to q^2/V^2, and therefore the variation of yield Y also reflects the variation of Y with the primary ion charge state. It has been found in many cases that $Y \propto \left(\frac{dE}{dX}\right)^2$ in the increasing part of the yield curve. When the velocity exceeds that corresponding to the maximum of the yield curve ($\simeq$ 1.1 cm/nsec) there is no simple relation between the yield and the energy loss. In addition, the maximum yield appears at a PI velocity that is lower that the velocity at which maximum dE/dx occurs.

More interesting information is obtained from experiments in which the parameter incident-charge-state q_i is varied. Before going into more details, let us consider how the charge state of a fast ion varies when it enters a solid material.

II.3. P.I. charge state dependence

Fast ions traveling in a solid rapidly reach highly excited states. Several processes can change the ionic charge state of an ion moving through the solid. Theoretically, several approximations must be made to estimate charge state values of a moving ion in a solid and experiments able to "photograph" the ionic charge state value in matter do not exist. However, we will describe in the next chapter an experiment that gives information on the charge variation inside solids.

After an ion has penetrated a certain distance x below the surface of a solid, its charge state reaches an "equilibrium value" $\langle q_{eq} \rangle$. An example of variation of charge state in a solid is shown by Fig. 4 which presents Kr at 1 MeV/u traveling through carbon. It must be noted that for heavier PI, like ^{127}I, the equilibrium charge state is preceeded by a pre-equilibrium charge state (see following chapter).

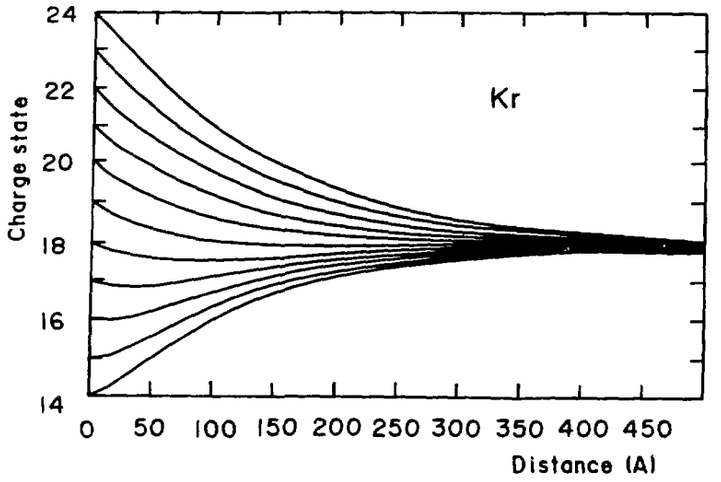

Figure 4
Calculated variation of the ionization state of Kr ions at 1 MeV/u passing through carbon material.

As seen in Fig. 4, ^{24+}Kr becomes ^{21+}Kr after 100 Å and ^{19+}Kr at 200 Å. The equilibrium value 18^+ is reached beyond 450 Å. This curve has been calculated by Maynard [25]. Several semi-empirical formulas are generally employed to calculate the equilibrium charge state value of a given projectile in a

given material [26,27]. Shima and collaborators [28] have established a semi-empirical relation that gives satisfactory values of equilibrium charge state :

$$q_{Shima} = Z_1 \left[1 - \exp\left(-1.25x+0.32x^2-0.11x^3\right)\right] \cdot \left[1 - 0.0019(Z_2-6)\,x+10^{-5}(Z_2-6)^2 x\right]$$

with $x = \frac{v}{v_0 Z_1^{0.45}}$, $v_0 = 3.6.10^8$ m/s and Z_1 and Z_2 are atomic numbers of projectiles target.

It is obvious from the expression dE/dx that the energy loss in the solid is proportional to $\langle q_{eq} \rangle^2$ once the $\langle q_{eq} \rangle$ value is reached. But what takes place before this state is reached ? It happens that the charge state does vary along the path of the primary ion (according to Fig. 4 for example for Kr in carbon) and that the energy loss dE/dx is essentially proportional to $q^2_i(x)$. $q_i(x)$ is the value of the ionic charge state for an initial charge state q_1 after a penetration of a distance x in the solid. Since an equilibrium value is reached within a few hundreds Angströms, the ion velocity does not change but, as seen above, the charge state and therefore the dE/dx can change enormously.

Reality is not as simple because there exists, inside the solid and outside the solid, a charge distribution. For energy loss estimation, the mean charge state is generally considered.

Instead of using the results of Maynard's calculation, it is possible (for atomic number below ≃ 40) to calculate q(x) with an exponential dependence proposed by Bohr [29] :

$$q(x) - q_{eq} = (q_0 - q_{eq}) \exp - \frac{x}{d}$$

where q_0 is the initial charge state, q_{eq} the equilibrium charge state, x the distance below the surface in Angströms, and d the distance of relaxation to equilibrium.

A fast PI ion with a charge state 30^+ deposits in the first 100 or 200 Å of a solid more energy than the same PI with a charge state of only 10^+. As a consequence, it is obvious that since energy losses are different, yields of secondary ions emitted from the surface are also different. Fig. 5 illustrates this charge state dependence. The material was a thin organic film of the molecule phenylalanine ($C_9H_{11}O_2N_4$, mw = 165). The incident charge state of the

primary ion Ar at 1 MeV/u was varied between 7 and 17. For Ar, the equilibrium charge state at 1 MeV/u is around 12.

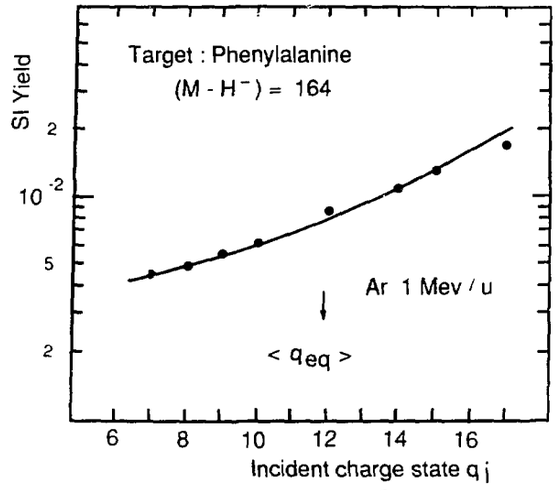

Figure 5
Variation of the emission yield as function of the incident charge state of Ar projectiles at 1 MeV/u.

The charge state of an Ar^{q_i} ion with $q_i = 7$ increases as the ion penetrates in the solid. Therefore, the SI yield corresponding to $q_i = 7$ includes also effects of energy dissipation inside the solid with larger charge state. If the incident charge state is 16^+, the charge state inside decreases and the SI yield includes effects of dE/dx with smaller charge state. Interactions below the surface contribute to a smaller rate of variation of $Y_{SI} = f(q_i)$. Projectiles with a smaller atomic number like ^{20}Ne or a larger atomic number like ^{84}Kr have different equilibrium charge state values. They generate respectively smaller and larger SI yield than Ar PI. Fig. 6 shows the results.

A large number of different primary ions has been used in Orsay and Darmstadt. Fig. 7 summarizes the results. It is observed that different PI with the same incident charge state and the same velocity provide different values of SI yield. The reason is that their charge states vary in a different way below the surface and contribute to a different amount of energy deposited in the solid.

Fig. 8 shows clearly how the charge state of 3 different ions Ne, Ar and Kr, with the same initial charge state 10^+, varies in a carbon foil.

An attempt has been made to reproduce the variation of the relative SI yields as a function of the incident charge state [30,31]. This is independant of any model of energy transfer but it is supposed that there is a contribution of the energy deposited at the depth x below the surface. Thus, at this distance x, the contribution to the total yield depends on the charge state variation $q(x) = f(q_i,x)$. Let us call $\frac{dE}{dx}(x,q_i)$ the energy deposited at x, then the contribution dY(x) to the yield at x can be written as :

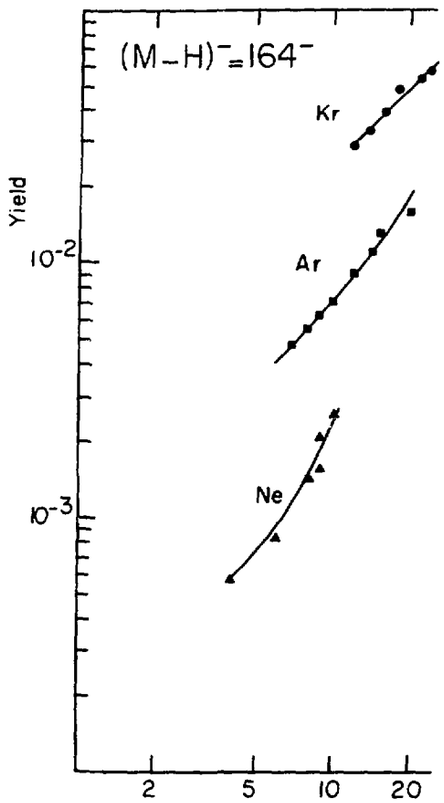

Figure 6
Relative yield of $(M-H)^-$ for the projectiles Kr, Ar, Ne at the same velocity (1 MeV/u) as function of their incident charge state.

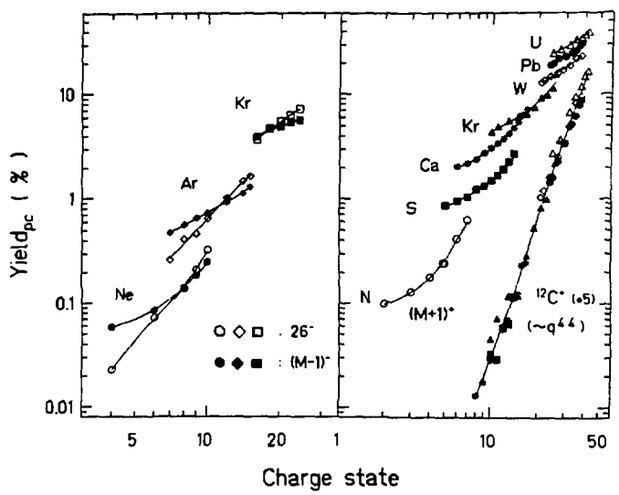

Figure 7
Similar results as in Fig. 6 for different projectiles. Results from the right part have been obtained in Darmstadt (K.Wien et al).

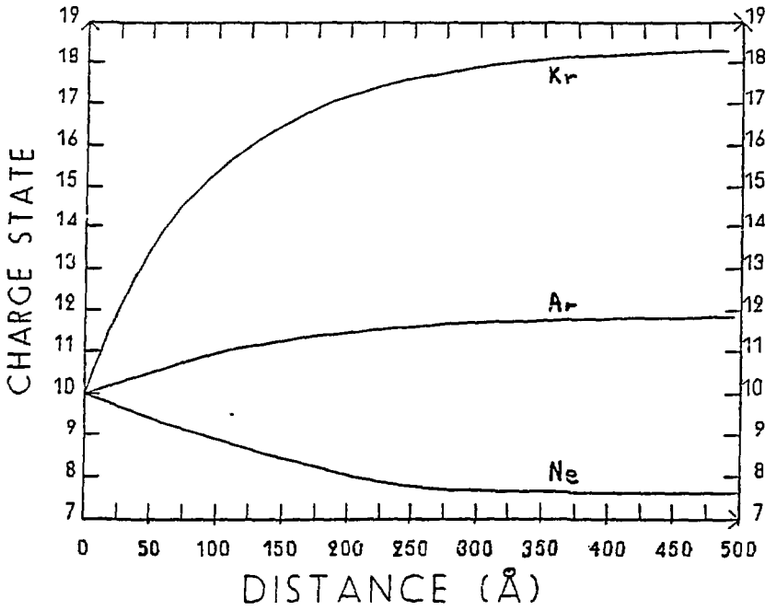

Figure 8
Calculated variation of the ionization for three ions (Ne, Ar, Kr) at the same velocity entering a carbon foil with a charge state 10^+.

$$dY(x) = A \left[\frac{dE}{dx}(x,q_i)\right]^n \psi(x)\, dx$$

A step function $\psi(x) = \left[1 + \exp\left(\frac{x-d}{\Delta d}\right)^{-1}\right]$, where d is an interaction depth that depends on $\frac{dE}{dx}$ values, has been used to characterize the desorption probability at a distance x. We have assumed the relation $d = B\left[\frac{dE}{dx}(q_i,x)\right]^{n'}$ with $\Delta d = 0{,}1\ d$. Therefore one gets :

$$Y_{q_i} = A \int \left[\frac{dE}{dx}(x,q_i)\right]^n \times \left[\frac{1 + \exp\left(x - B\left(\frac{dE}{dx}(q_i,x)\right)^{n'}\right)}{0{,}1\ B\left(\frac{dE}{dx}(q_i,x)\right)^{n'}}\right] \qquad (1)$$

If $q_i = q_{eq} = cte$, we obtain $Y_{q_{eq}} = A.B.(q_{eq})^{n+n'}$.

In Fig. 9 the fit of the shape of one curve (Kr for example) allows us to obtain values of B and n'. From the experimental relationship

$$Y_{q_{(eq)}} \propto C\, q_{eq}^{\,n+n'}$$

deduced from Fig. 9, we obtained n+n' and C = AB. These parameters are the same for any primary ions on the same target n' values are generally around 1/2 and n values around 2.

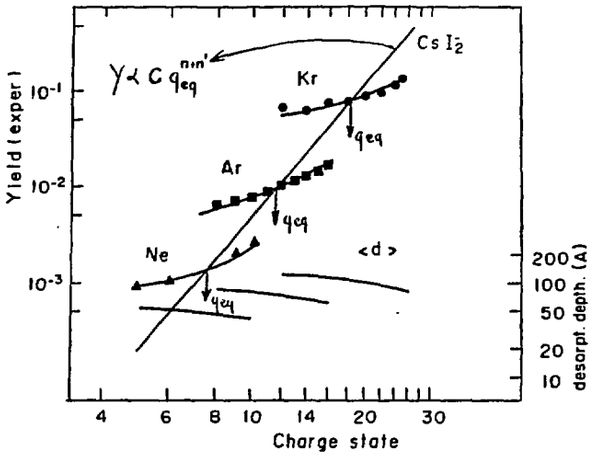

Figure 9 : Experimental and calculated curves for $q_{eq} \Rightarrow Y \propto C\ q(eq)^{n+n'}$.

This approach is a phenomenological approach and does not explain the basic processes. It however indicates that there is a certain interaction depth in the desorption processes and that the energy deposited inside plays a role in the desorption processes. All of the preceding is valid for molecular ions and atomic or cluster ions emitted from a film of material. Interaction depths of 90 ± 20 Å and 300 ± 80 Å for ^{32}S and ^{127}I have been estimated by this procedure. During these studies on SI by multiply charged ions, angles of impact have been varied as well as thicknesses of material.

II.4. Depth of emission

The increase of secondary yields with the thickness of samples was first been studied with fission fragments from ^{252}Cf [32]. These experiments have shown that intact molecular ions can be emitted from underneath the upper layers. Recently, Langmuir-Blodgett (LB) films have been used to obtain quantitative results as function of the sample thickness [33,34]. These results were consistent with a simple picture of emission from a "crater" with a depth of about 200 Å.

Experiments with beams of ^{32}S and ^{127}I at 1 MeV/u, in their equilibrium charge states were used to bombard L.B. layers of nM_1 on $n'M_2$. The number of top layers n has been varied from 2 to 12. Molecular ion yields from upper and underlying layers were measured simultaneously for each target. Fig. 10 shows the results for $^{127}I^{24+}$ projectiles for n' = 6 layers. The yield of the top layer saturates at $n \simeq 10$ and the yield from the "bottom" layer decreases.

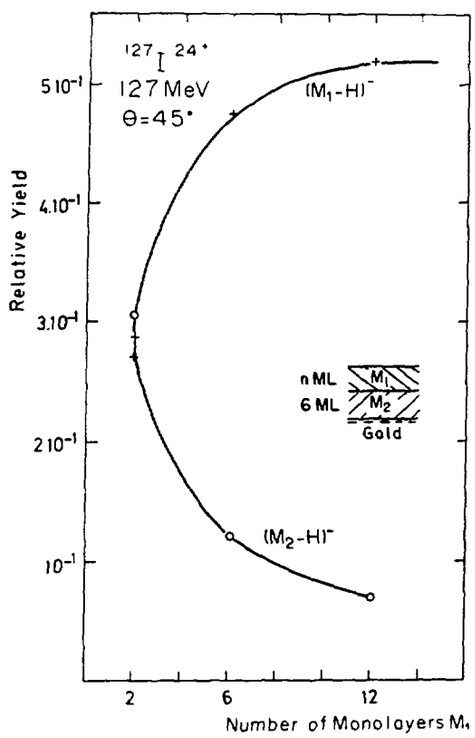

Figure 10
Yield variation from the top layer and bottom layer molecular ions as function of the number of top layers.

The saturation depth is rougly the same with ^{32}S and ^{127}I although the electronic stopping power of the projectiles are different

$$\left(\frac{dE}{dx}\,^{127}I \simeq 3\,\frac{dE}{dx}\,^{32}S\right).$$

The absolute secondary ion yield of emission is, however, 10 times larger with ^{127}I than ^{32}S. That is consistent with many other experiments where a $(dE/dx)^n$ dependence of secondary ion yields with $n \simeq 2 - 3$ is reported [35]. If we apply the simple picture of crater emission (conical volume for example), the cone would have the same depth for ^{32}S and ^{127}I but a larger surface cross section in the case of ^{127}I ions, which have a higher dE/dx value.

II.5. Incident angle dependence of the electronic desorption yield [36]

Experiments with different incident charge states and different angles of impact have been performed. The charge state effect has been described previously, but here we also varied the angles θ. Fig. 11 shows an example of results for a LB target made of two different kinds of molecules. The beam was ^{127}I at 127 MeV. For an impact angle of 20°, the charge state effect is clearly visible while at grazing angle, around 78°, there is no effect of charge state. At 20° the slope of yield variation with q_1 (incident charge state) is very steep. The deposited energy loss that contributes to the SI emission depends on the charge state variations along the track. Qualitatively, at this angle, the interaction distance (see above) is at least of the order of the distance traveled for equilibration (200-300 Å). As θ increases, the influence of the primary ion charge state vanishes and the yield tends to be flat. The PI travels a long distance (close to the surface) compared to the equilibrium charge state distance, and consequently, the secondary emission depends mainly

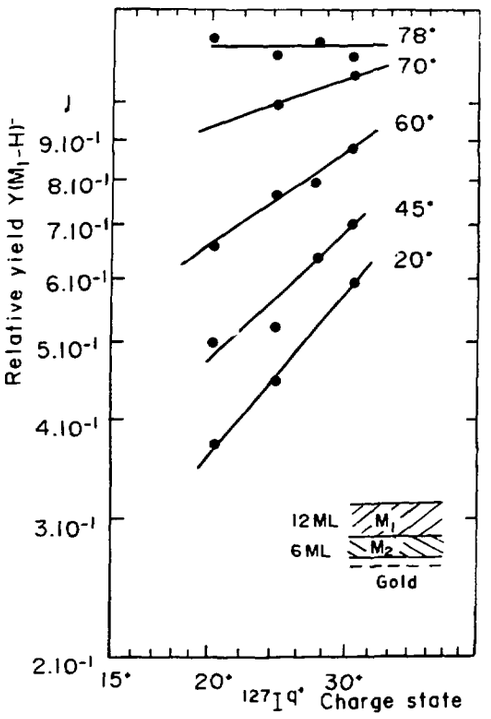

Figure 11

Experimental yield of the molecular ions M-H⁻ as function of the angle of incidence and the charge state of the primary ions of ^{127}I at 127 MeV.

on the energy loss with the charge state equilibrated. The memory of the incident charge state is lost. The geometrical shape of the volume of emission is expected to vary considerably with the angle of projectile impact and is probably very asymmetric for larger angles.

Others results have been shown in reference [36]. A shock wave model or a pressure pulse model was used to tentatively reproduce the data. Reasonable qualitative agreement was obtained.

These results also show that, with MeV ions, a simple relationship between the emission yield and the angle of impact does not exist. $Y = f(\theta)$ depends on the incident charge state.

All the results presented above have been obtained with secondary ions. Will they be the same for neutral species emitted from the surface ? This is a very important question because in all theoretical models the ionization step is not treated. There is therefore a need for new experimental results on neutral emission. These experiments might be more difficult, but they are necessary to confirm that the observation of secondary ions does not give a false picture of the general mechanism of emission.

Some experiments with neutrals have already been performed by the Uppsala Group [37,38].

Desorption models have been developed by several groups, and it would be interesting to make a systematic comparison [see 37,38]. The general picture is that, during the passage of a fast ion through the solid, intense ionization and excitation occurs in and just outside the nuclear track. Electrons carry energy far into the material ; the electronic excitation density is

assumed to decrease as 1/r with the distance r from the track. This fast process ($\simeq 10^{-15}$ sec) must generate a coherent transfer of momentum to the volume of molecules that escape from the bulk. The angular distribution of emitted molecules is asymmetric with respect to the primary ion trajectory [39]. This strongly favors a fluid dynamical model.

There is a long time delay between the electronic energy deposition in the solid (a fast ion travels 10 Å in 10^{-16} sec) and the molecular ion emission. Molecular vibration and expansion take 10^{-12}-10^{-13} sec ; therefore molecules are ejected into vacuum 3 or 4 orders of magnitude later. During all this time, a large number of complex processes take place in the material. Experimental access to these intermediate phenomena is very difficult.

However, at the very beginning of the interaction, shortly after the passage of the PI, light ions like H^+ or fragments like $^{12}C^+$ are emitted from the solid surface and the study of their emission has been applied to various problems (see IV).

III. EMISSION OF HYDROGEN IONS FROM SOLID SURFACES

In experiments using multiply charged MeV ions as projectiles, it has been shown that H^+ ion emission follows a very simple pattern. For a given projectile velocity the emission yield of H^+ is independent of the bombarding ion and therefore of the total energy lost in the foil. It depends only on the primary ion charge state when it crosses the surface, and not on the charge state variation below the surface. Fig. 12 shows the yield variation of H^+ for

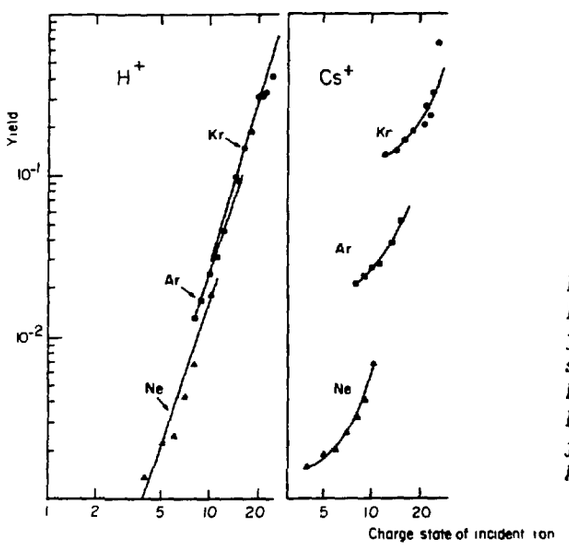

Figure 12
Left side : variation of H^+ yield with the incident charge state of the three projectiles Ne, Ar, Kr.
Right side : variation of Cs^+ from a CsI deposit. A very marked difference is seen.

projectiles of Ne, Ar, and Kr at 1 MeV/u. At the same incident charge state, the same yield values are obtained. For comparison the yield of Cs^+ from a CsI sample is also shown. Another example is given in Fig. 13 with Au and I projectiles at 0.5 MeV/u. There is an overlapp of charge states between 22^+ and 27^+. H^+ yields are also the same. An application of this experimental observation has been to use the value of the H^+ yield to measure the incident charge state of fast projectiles.

To investigate the role of the charge state on H^+ ion emission, primary ions with a much lower energy have been used [40,41], for example Tl^q ions at 110 keV ($\simeq$ 0.5 keV/u, i.e. 1000 times less of energy) and Ar^q at 18 keV. In order to be able to compare MeV ions and keV ions, the measurements were performed under exactly the same experimental conditions, i.e., with the same target and in the same reaction chamber continuously kept under vacuum. Only the projectiles were changed.

Fig. 14 shows the experimental set up. A thin target foil was positioned in the center of the reaction chamber. Ions of Au and I at 0.5 MeV/u were obtained from the Tandem machine. The charge selection was made by a magnet prior to the target. Multiply charged keV ions were obtained from a small alpha radioactive source. Let us describe the experimental arrangement. It is easy to obtain multicharged MeV ion from accelerators. It is not as common to generate 100 keV ions multiply charged. As an ion source we have used recoiling atoms resulting from radioactive alpha decays of ^{212}Po and ^{212}Bi. It is easy to prepare radioactive sources of thoron emanation on thin gold or aluminium foils. The radioactive decay serie leads to ^{212}Po and ^{212}Bi, which are

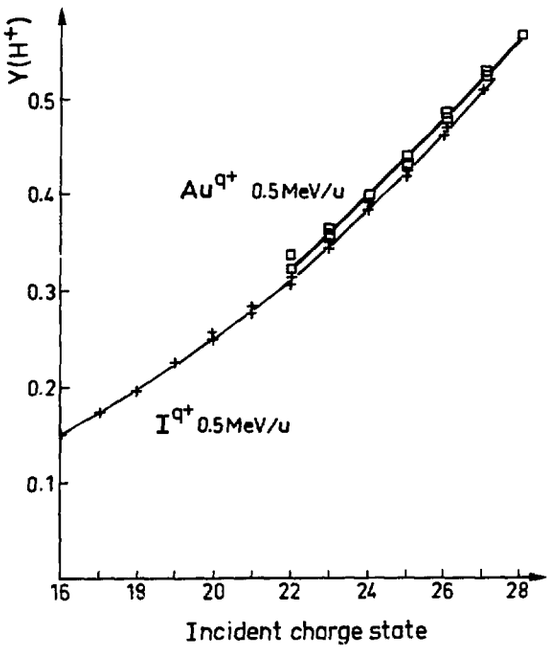

Figure 13
Emission of H^+ ions from the surface of the same carbon foil bombarded with ^{127}I and ^{197}Au at the same velocity.

alpha emitters. ^{212}Po emits an 8.78 MeV α particle and ^{212}Bi a 6.05 MeV α particle. For every α emission there is a recoiling nucleus with an energy $E_{recoil} = 4\ E_{\alpha}/208$. Due to the internal conversion of the 39.8 keV gamma ray, a charge state distribution of Tl atoms is generated and can be measured by time of flight.

It is therefore rather easy and simple to generate multicharged keV ions. In Fig. 14, an α source is mounted at 20 cm from the target. A recoiling atom with a certain charge state is associated with each α decay and the α particle is detected by a silicon detector that provides a start signal. The recoiling nuclei is accelerated by the difference in potential applied between the source (3 to 8 keV) and a 98 % transmission grid at zero potential. A thin grid (at ground) is placed 3 mm from the target surface, which itself is at the same potential as the source. Because of the different charge states, the accelerated recoils have different energies, and the measurement of their TOF between the source and the target allows clearly separation of the different

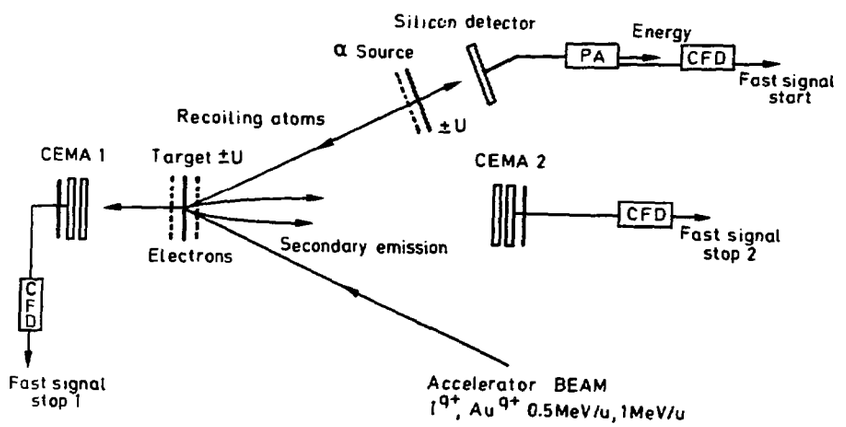

Figure 14

Experimental arrangement for the bombardment of the same target with projectiles at 0.5 MeV/u and 0.5 keV/u.

charge states that appear as peaks in Fig. 15. The charge state of each incident ion hitting the target is thus identified and selected. It is an event by event experiment. The TOF of the correlated secondary ions are accumulated in different computer memories according to the selected charge state.

In Fig. 14, keV ions and MeV ions are shot at the target at an angle of 25°. Where do H^+ ions come from ? Hydrogen, water, organic contaminants at the surface ?

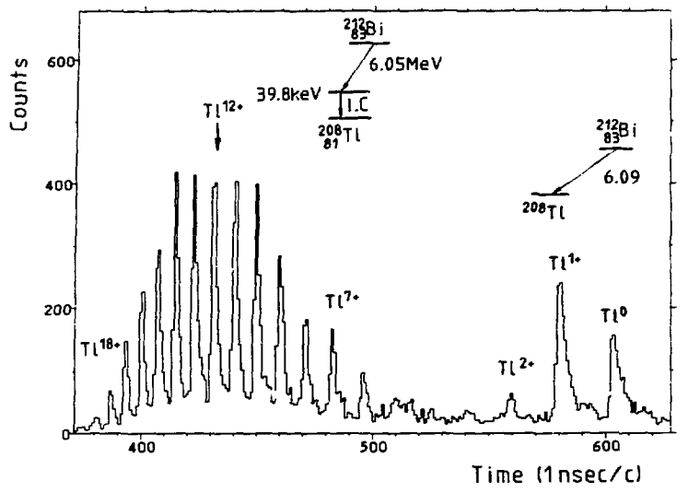

Figure 15
Charge state distributions of the primary ions of ^{208}Tl measured by time of flight.

A mass spectrum recorded just after cleaning the foil by sputtering with Ar ions from and Ar gun did not exhibit any H^+ lines. However, after a few minutes, H^+ ions were present again and the yield saturated after 10 minutes. Negative ions at $16(O^-)$ and $17(OH^-)$ were also present in the negative spectra. This indicates the presence of water at the surface.

After heating a UHV system (at Texas A&M) and cleaning the target, a very small amount of D_2O was introduced in the chamber. Almost immediately, ion peaks of D_1^+, D_2^+, D_3^+ were observed in the mass spectra [42].

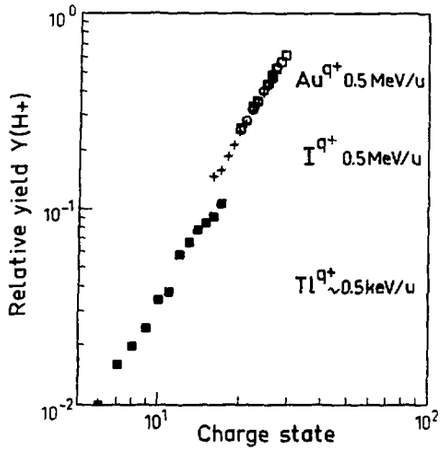

Figure 16
Relative yield of H^+ with three projectiles as function of their incident charge state.

Fig. 16 shows results obtained on H^+ yield as a function of the incident charge state for the three types of projectiles (Au and I as shown before) and ^{205}Tl. It is observed that for Tl ions having an energy 1000 times smaller ($v = 3.10^7$ cm/sec), the emission yield of H^+ remains about the same. The trend in the variation is the same, and in all cases a power law $Y(H^+) \propto q_1^3$ has been established.

There is no direct evaluation of the mechanism of emission. It has been emphasized that when a multiply charged ion approaches a surface at a velocity about 2.10^7 cm/sec, a large number of electrons are captured in outer shells at distances 25-50 Å from the surface [43]. Auger cascades occur in the decay processes. The time for the first step of the cascade is around 10^{-14} - 10^{-15} sec and X rays are emitted once the projectile has reached the surface. The triggering process of H^+ emission occurs before any charge state variation, and the question is wether or not the mechanisms are the same for keV and MeV ions. It is only within the first ten Angströms through the solid that electron losses and captures change the ionization state of fast ions, and these 10 Å are traveled in 10^{-16} sec. This gives a time scale of 10^{-16} sec for the triggering process.

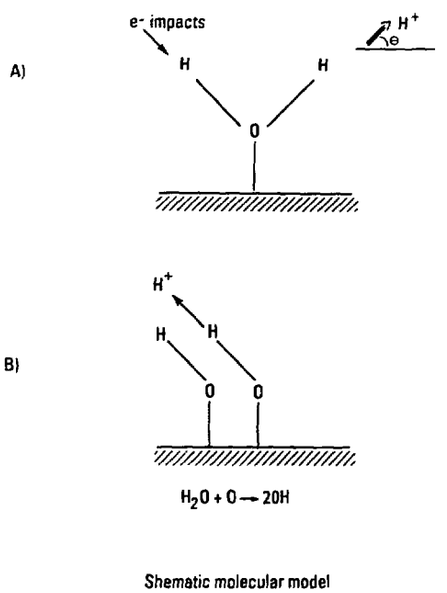

Figure 17 : Shematic molecular representation of attachment.

When a large charge state approaches a surface, electrons are ejected from the surface. In keV experiments, as said before, it seems that electrons escape from the surface before impact, and it could happen that the projectile is partially neutralized before hitting the surface. In any case, fast displacements of electrons take place at the surface where water molecules are attached. Electronic excitation of a surface molecular bond can occur in 10^{-16} sec. Excited states can be repulsive and the electronic energy (≃ coulomb energy) can be converted into nuclear motion along the direction of the bond that is ruptured. This picture is used to explain the preferential direction of emission of fragments from small molecules adsorbed at surfaces and "desorbed" by electron impact (ESD = electron stimulated desorption). Fig. 17 shows one type of attachment of a water molecule to a surface. Angular distribution mea-

surements of emitted H^+ can give information on bonding to the surface as well as on molecular structure [44].

In our case the primary charged particles arrive at a certain angle θ. Electron displacement at the surface could excite surface bonding states and interatomic bonding states. With well known surface structures (in ultra high vacuum) it would be interesting to perform experiments similar to ESD experiments and verify if angular distributions of H^+ emission would yield information on molecular bonding.

It is likely that a local positive electric charge results from the electronic emission (with keV and MeV ions). A rather strong coulomb respulsion can therefore accelerate the H^+ ions. This would explained the H^+ energy distribution that has an average value around 7-8 eV and that extends to large value (≃ 20 eV). Several groups have measured H^+ energy distribution with fission fragments or ion beams [45-49]. A coulomb repulsion model is proposed by the Uppsala group [49]. The q^3 dependence of the H^+ emission yield can also be explained by a coulomb repulsion [50].

No energy measurement has been made for low energy multiply charged projectiles. This is obviously one of the experiments to be made. In addition, the initial energy measurement of H^+ as a function of the primary ion charge state is also another (or simultaneous) experiment to be performed. Light secondary ions like D^+ should also be used.

A first test experiment was tried at Orsay with a ^{127}I beam at 1 MeV/u but the results were not satisfactory. However, it seems that H^+ ions of higher energy are ejected by more highly charged projectiles. This should be repeated with keV and MeV ions because, if the mechanisms of emission are similar with keV and MeV projectiles, the energy spectra should, of course, be the same.

IV. APPLICATIONS OF THE PHYSICS OF EMISSION OF H^+ TO THE DETERMINATION OF EQUILIBRIUM (AND PREEQUILIBRIUM) CHARGE STATE OF A FAST IONS IN A SOLID

The behavior of the charge states of energetic ions passing through matter is a difficult problem of considerable theoretical interest. Energy losses in solid and gas depend on charge state and on its variation in the first layers in the case of desorption. Energy loss measurements in plasma are being made in several laboratories in connection with basic aspects of fusion indu-

ced by fast heavy ions [51] leading to a renewal of activity for these questions.

One of the questions raised a long time ago by Betz was : Is there a difference of ionic projectile charge states inside and outside stripper targets ? This question deals with electron loss and gain in the solid, excitation time, and differences of equilibrium charge states between gas and solids. According to Betz and Grodzins [52], Auger transitions take place once the ion leaves the exit surface of a target. This process of deexcitation from multiexcited states that are populated inside the solid would account for the enhancement of the projectile charge state after passage through a solid target. Until now, the equilibrium charge state of a fast ion was determined by means of a magnetic spectrometer after the beam had passed the target. This means that the ions have traveled for a long time in vacuum after exiting from the surface.

Since the yield of H^+ is strongly dependent on the charge state of the projectile, this yield has been used, after calibration, as a sensitive probe of projectile charge state at the surface.

Fig. 18 illustrates the experimental setup. Several targets can be successively put in the irradiation position without opening the vacuum chamber. The target and the MCP detectors are mounted on a rotating platform. Therefore the beam can bombard the same target surface either directly or from the back after passage through the target. In both cases the secondary ions originate from the same area. About 70 cm upstream from the target, a foil (equilibrium charge state foil) of the same nature and thickness as the target can be inserted into the beam. At the highest beam velocity used (corresponding to 1.5 MeV/u) the time of flight of an ion projectile is about 40 nsec.

In the "Secondary Ion TOF chamber" carbon foils of 20-40 $\mu g/cm^2$ and gold foils of 170 $\mu g/cm^2$ are also used. For charge state measurements inside a solid, very thin foils of nitrocellulose have been prepared as targets (100 Å to 500 Å).

The experimental procedure is as follows :

i) Measurement of the calibration yield curve $Y(H^+) = f(q_1)$. For each incident charge state the H^+ yield per incident ion is measured, for example curve 1 in Fig. 19.

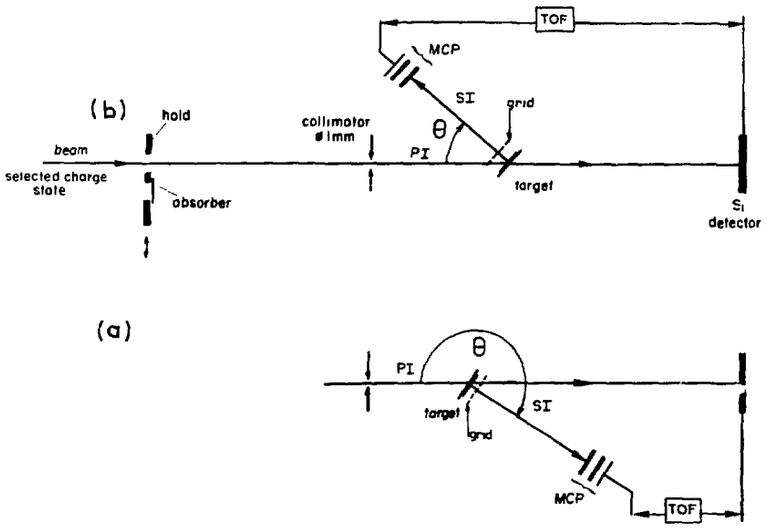

Figure 18
Experimental arrangement for charge state measurements of fast ions in solids (Tandem Orsay).

ii) In a second series of measurements, the "equilibrium charge state foil" is inserted into the beam and the H^+ yield (from the same point of the target) is again measured as a function of the incident charge state hitting the equilibrium charge state foil. If the equilibrium charge state is reached in this foil the H^+ yield curve exhibits a flat dependence versus the charge

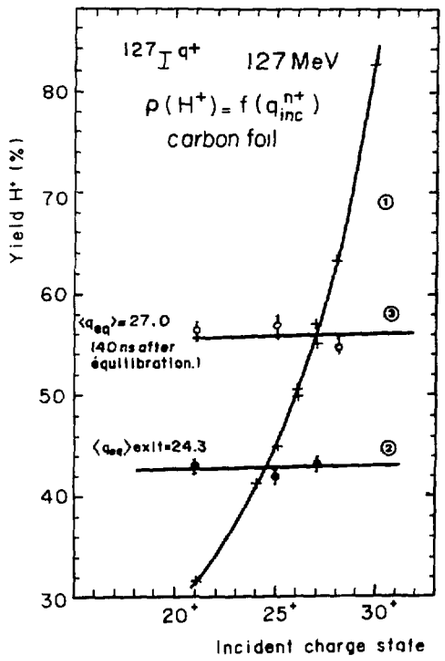

Figure 19
Experimental results on equilibrium charge states (see text).

state. This is shown with curve 3 in Fig. 19. The intersection between curve 1 and 3 gives the equilibrium charge state of an ion more than 40 nsec after passage through a solid foil ("$<q_{eq}>$" in the figure).

iii) The third step is to turn the target by 180°, remove the "equilibrium charge state foil", and measure once more the H^+ yield curve as a function of incident charge states. Results are shown in curve 2 in Fig. 19.

The crossing between curve 1 and 2 gives the equilibrium charge state measured at the exit surface of the target when the projectile leaves the surface ("$<q_{eq}>$ exit" in the figures). The results from Fig. 19 indicate that the charge state at the exit surface is smaller than the charge state measured more than 40 nsec later. When the target is thick enough to achieve charge state equilibrium, the H^+ yield measured at the exit surface does not depend on the projectile charge state at the entrance surface and $Y(H^+)_{exit} = f(q_i)$ is flat as shown by curve 2 in Fig. 19. This means that the memory of the entrance charge state is lost. If, however, the target thickness is smaller than the equilibrium distance, the equilibrium charge state is not reached, and the H^+ yield increases with q_i. This case will be shown in the following section where very thin targets are used. The experimental yields were reproducible, their values being checked several times. During the experiments, the target chamber was not opened to air, all the targets were then kept under vacuum.

As demonstrated in Fig. 19, outside a carbon foil the equilibrium charges states $<q_{eq}>$ of ^{127}I was found to be 27 whereas inside the foil $<q_{eq}>$ exit is only 24.3. These values are average values which have not been corrected for the charge state distribution. However, based on the calibration curve $Y(H^+)$ which varies as q^3, and the shape of the charge state distributions [53], we have calculated that the mean equilibrium charge state values extracted from the present results are overestimated by only a few percent.

Several different ion beams and targets have been investigated by using the H^+ method. The increase of charge state of a fast ion traveling through a foil is observed for projectiles with masses above 40. Let us recall that equilibrium charge states in gases are smaller than those in solids [54]. For example, ^{127}I at 110 MeV the difference between a gas and a carbon target is about 7 charge units. The post foil increase is only about 3 charge units, and in general the increase $\Delta\bar{q}$ is only 10-15 % of the equilibrium charge at the exit surface of a solid. Therefore only part of the difference between gases and solids can be due to post-deexcitation. Fig. 20 is a schematic view of charge state variation inside and outside solid targets according to Bohr and Lindhard [55], Betz and Grodzins [52], and experimental results [53].

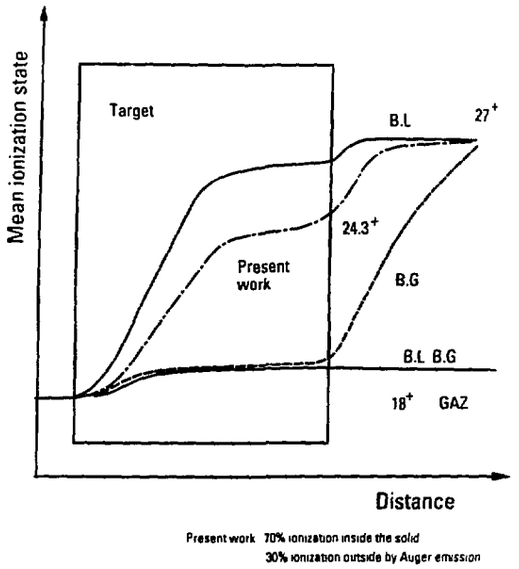

Figure 20
Shematic representation of charge state variation inside and outside a target.
- *Bohr and Linhard theory (BL)*
- *Present experimental result*
- *Betz and Grodzins (BG).*

The variation in a gas target is also given.

Experimental and theoretical mean equilibrium charge states are presented in ref. [53].

Theoretical calculations of charge states inside matter have been pursued by G.Maynard and C.Deutsch [25] who have considered an average atom model with 10 levels of number quantum n populated by Pn electrons. The mean ionization states <q> can be written as :

$$\langle q \rangle = Z - \sum_{n1}^{n=10} Pn \qquad \text{and} \qquad \frac{d\langle q \rangle}{dt} = - \sum_{n1}^{n=1} Pn$$

$$\text{with } P_n = - P_n \left[l(n+n) + \sum_{k \neq n} (2k^2 - P_k)\, l\,(n,k) \right] + (2n^2 - P_n) \left[g(n,n) \right]$$

$$+ \sum_{k \neq n} P_k \, g(k,n)$$

where, if $k \neq n$, $l(n,k) = g(n,k)$ represents the rate coefficient for one electron transfer from level n to k ; g(n,n) and l(n,n) are rate coefficient for recombination and ionization [25]. The rate of shell occupancy or vacancy varies differently for the different shells, as a function of time (and of distance). In other words the hole population is taken into account. Therefore, according to the total shell population probability, the total ionization state can be represented by the calculated curves of Fig. 21 for ^{127}I projectiles at 1 MeV/u passing through a carbon foil. To verify the prediction, experiments based on H^+ yield measurements at the exit surface of thin foils have been performed. This procedure allows the charge state of a projectile to be determined after a certain thickness of material.

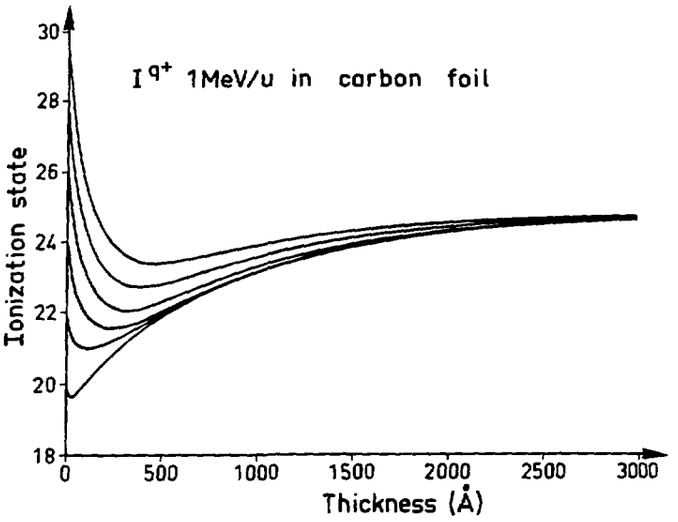

Figure 21
Theoretical predictions for the charge state variation inside a carbon foil of a ^{127}I projectile.

By changing the thickness, it is therefore possible to determine mean ionization charge states as a function of the distance traversed. Self supported targets of carbon foils from 250 to 4000 Angströms have been bombarded by primary ions with charge states selected by a magnet (between 19 and 28). Fig. 22 shows the experimental variation of the ionization state of ^{127}I. It is shown that whatever the initial ionization state, a common value is reached

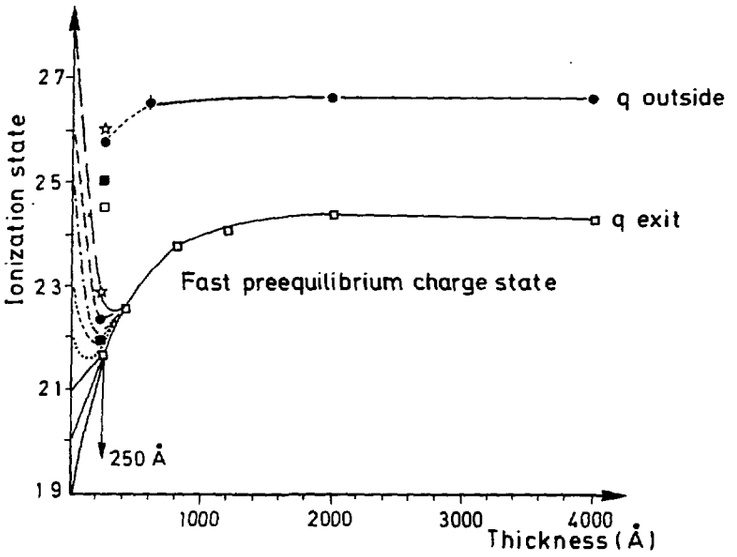

Figure 22
Experimental ionization state variation of ^{127}I in carbon.

after 400-500 Angströms (pre-equilibrium charge state). The memory of the entrance channel is lost, but the complete charge state equilibration is not yet reached. This is clearly observed in Fig. 22 where the charge state increases beyong 500 Å. Full equilibration is attained at about 2000 Angströms.

These experiments are the first ones to give information on variation of charge state in matter. Others measurements with different projectiles and targets would facilitate a comparison with theoretical models and refine our understanding of complex collisions and excitation in solids. This example shows that ion desorption phenomena have been unexpectedly applied to another field in physics.

V. FROM SINGLE ATOMS TO CLUSTER IONS AS PROJECTILES

KeV ions have been used for many years as projectiles to produce secondary ions from inorganic surfaces. It is only since the past decade that this method of producing ions from non volatile samples has been used for organic solids [56]. With polyatomic ions as projectiles, an enhancement of the secondary ion yield was observed when compared to single atom ions [57-62].

A systematic study of secondary ion yields from different targets bombarded by various projectiles has been undertaken at our laboratory, following the first experiments performed by the Uppsala and Texas Groups [63,64]. The experimental method has been much improved. Organic molecular ions, polyatomic ions like CsI clusters and metallic clusters of gold have been used as projectiles. Table 1 shows the different projectiles and targets. Bombarding energies were between a few keV and 56 keV.

Fig. 23 shows the experimental set-up for organic and CsI cluster projectiles. These are produced from a compound deposited on a thin foil and desorbed by impact of one of the fission fragments. The other fission fragment is detected and activates the timing electronics. These "primary ions" are accelerated by the potential U_1 and strike a target after a free field distance. Upon impact, secondary ions and electrons are emitted from the target. Electrons are very fast and therefore, the time between the spontaneous fission events and the impact of electrons at MCP2 (see Fig. 23) gives the TOF of primary ions.

PRIMARY IONS

ORGANIC PROJECTILES

MASS	COMPOUND
73^+	$(CH_3)Si^+$
147^+	$(CH_3)_3SiOSi(CH_3)_2^+$
120^+	$M - COOH^+$ fragment of phenylalanine
166^+	$[C_6 H_5 CH_2 CH(NH_2)COOH+H]^+$ phenylalanine
331^+	$(2M+H)^+$ phenylalanine dimer
300^+	$C_{24} H_{12}^+$ coronene
598^+	$2(M-H)^+$ coronene dimer

ATOMIC AND CLUSTER PROJECTILES

Cs^+
Cs_2I^+
$Cs_3I_2^+$
} with CsI target and Cs ion gun

Au_n^+ n = 1 to 5 with Gold LMIS pulsed
Au_n^{++} n = 1 and 3

TARGETS

Gold

$R_4SiW_{12}O_{40}$

CsI

Organic films : Phenylalanine
Dinitrostilbene
Lipid EG
Erythromicin

ENERGY

5 keV < E_{impact} < 30 keV
60 keV for Au_n^{++}

Table 1

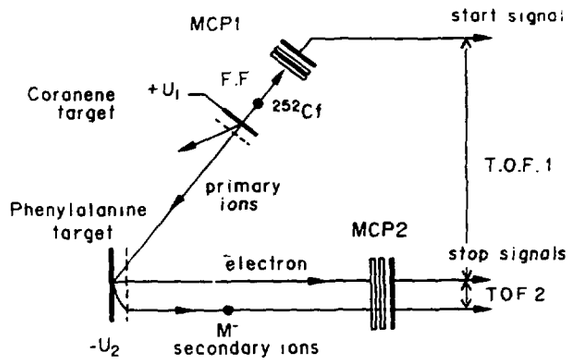

Figure 23
Experimental arrangement for impacts of large clusters produced by fission fragments.

Electronic coincidence window can be set on TOF 1 events (for example on a molecular ion TOF peak) and this time window serves as a t_0 marker for the time signals that are in the same event. An example is given in Fig. 24 a-b. Fig. 24 is the sum of primary ions and secondary ions. Fig. 24.b shows the SI spectrum of ions emitted by the impact of a molecule of mass 300 (coronene).

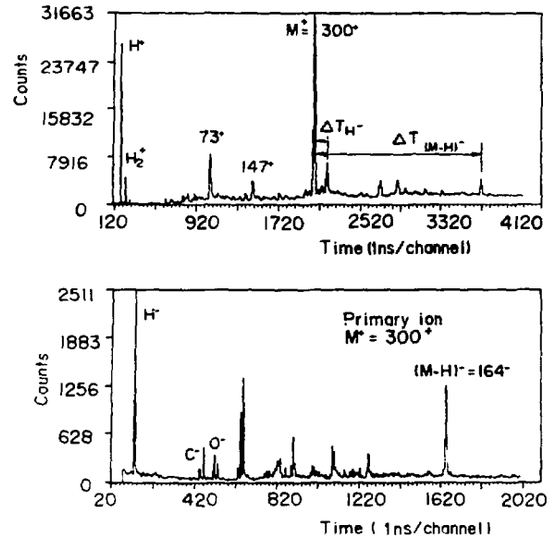

Figure 24
Cumulative time of flight spectrum (top).
Correlated time of flight spectrum obtained with a time window on M = 300.

The data acquisition system allows to define several time windows to be defined on TOF 1. The experiment is, of course, performed in an event by event mode. This allows the study of single projectile-target interactions. Results (from ref. 65) are presented in Fig. 25.a, which shows SI yield variations as a function of the cluster size and the energy per mass unit (keV/u). The trend of the data is higher yields for more complex primary ions. The yield of the molecular ion $M\text{-}H^-$ = 164 from the phenylalanine target increases by a factor

of 20 upon going from Cs^+ to Cs_2I^+. That is a yield enhancement of about 7. We define the yield enhancement factor ε for a homonuclear projectile A_n having n constituents by :

$$\varepsilon = \frac{Y\ A_n(E)}{nY\ A(E/n)}$$

where $Y\ A_n(E)$ is the secondary ion yield for the cluster projectile at energy E and $Y\ A(E/n)$ the yield for the constituent atom of the homonuclear projectile at equal velocity.

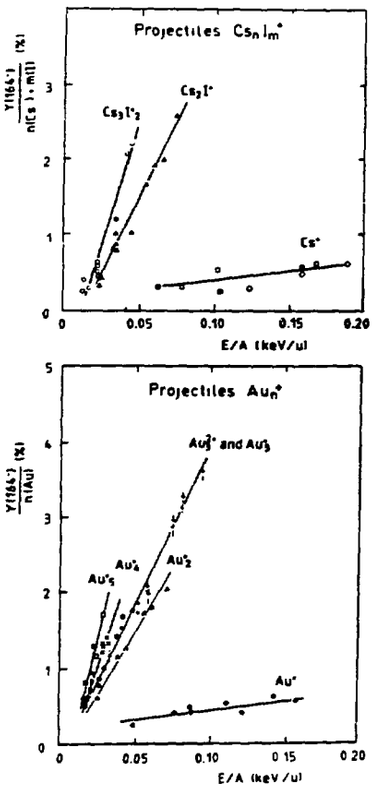

Figure 25
- *Relative yield per constituent of the cluster projectile as function of keV/u units ($\propto v^2$).*
- *The results with gold clusters have been obtained with a liquid metal ion source.*

Similar effects have been observed with clusters of gold atoms bombarding targets. In this case, a liquid metal ion source (LMIS) built by P. Sudraud and G. Ben Assayag [66] has been used[1]. A pulsation of the extracted focused beam allows easy identification, by time of flight measurements, of the different cluster ions produced in the source [67-68]. With a double pulsation it is possible to select a Au cluster of a given mass with which to bombard a

[1]The simple design for the ion source can be obtained from P.Sudraud, Orsay Physics, Orsay

target. The intensity of the ion source is adjusted to a small value in order to have only one or none primary ion per pulse. The exact number of cluster ions hitting the target surface can be accurately known. Fig. 25.b shows the variation of the molecular ion yield of $(M-H)^-$ from phenylalanine for the different projectiles Au_1, Au_2^+, Au_3^+, Au_4^+, Au_5^+ as function of keV/u.

Yield variation

The general trend of variation is very similar to that observed with CsI clusters. The variation of yield with the energy of impact is very steep and it would certainly be very interesting to increase the kinetic energy of those high mass clusters.

The three types of projectiles ; organic molecules (composed of light elements), ionic clusters (mass of constituent about 130), and gold clusters (mass of constituent equal to 197) all produce the same yield enhancements.

The SI yields are proportional to the square of the projectile velocity V and follow a power law of the number of cluster constituents n. This can be expressed with the following equation :

$$Y(SI) = K(SI).n^{\alpha}.V^2 \qquad (6)$$

- $\alpha = 2$ for SI atomic ions I^-, Au^- and organic fragments and molecules,
- $\alpha = 3$ for SI cluster as $(CsI)_n I^-$, $Au_k I_l^-$.

Let us consider the mass B of the constituent for a simple homonuclear cluster projectile B_n. We can write :

$$Y_{B_n}(SI) = k(B).n^2.B^2.V^2 = k(B).M^2.V^2 = k(B).P^2 \qquad (7)$$

Here, the constant k depends on the SI and the mass of the constituent of the cluster. In this case, the yield is proportional to the square of the projectile momentum P. This simple expression suggests that momentum plays a major role in the desorption process.

Although the processes of energy deposition by keV cluster ions and MeV ions are different, it is of interest to compare the desorption yields of both types of projectiles. The secondary ion emission reflects the amount of energy that is brought into the medium over a certain distance below the surface in an undefined volume after energy damping. A rough estimate indicates that for a fast ion (M = 100, E = 60 MeV) the amount of energy available for desorption is about 100 keV if one considers a desorption depth of 200 Å. On the other

hand, a gold cluster Au_6 with an energy of 60 keV deposits its energy over a distance between 150 and 200 Å. The linear energy loss values are thus not so different. Table 2 give a comparison of secondary ion yield between different cluster projectiles and fission fragments (F.F.) from ^{252}Cf. It is known that atomic ions in the keV energy regime are much less efficient than MeV ions for desorption-ionization (a factor of 20 to 100 less per projectile for organic compounds). It is interesting to note that gold clusters of Au_5 at 27 keV and Au_3^{2+} at 60 keV give secondary yield values close to those obtained with fission fragments for polyatomic samples. For a monoatomic target (Gold foil), cluster ions generate a much larger yield of Au^- than F.F.

P.I. / ENERGY / TARGET IONS	Au^+	Au_3^+	Au_5^+	Au_3^{2+}	FF ^{252}Cf
	27 KeV	27 keV	27 keV	60 KeV	0.5 MeV/u
LIPID EG MW = 528^-	7.10^{-4}	$0.87.10^{-2}$	$1.60.10^{-2}$	$\simeq 2.10^{-2}$	$\simeq 6.10^{-2}$
$R_4SiW_{12}O_{40}$ MW = 2821^- MW = 3086^-	$0.2.10^{-2}$ $0.15.10^{-2}$	$0.8.10^{-2}$ $0.4.10^{-2}$	$1.2.10^{-2}$ $0.6.10^{-2}$	$\simeq 1.6.10^{-2}$ $\simeq 1.10^{-2}$	$2.7.10^{-2}$ $2.2.10^{-2}$
GOLD MW^- = 197^-	6.10^{-3}	$1.3.10^{-2}$	2.10^{-2}	$2.6.10^{-2}$	$< 10^{-4}$

Table 2

A new project [69] for high energetic cluster ions is being prepared at the Orsay Institut. A large amount of energy could be deposited in a short time on a small area. As in the case of a laser, it is possible to calculate the "power density" for a fast molecular ion striking a surface. For example, a molecular ion of mass 20000 daltons (with a mean radius of 50 Å) at an energy of 4 MeV will deposit its energy in a time around 5.10^{-14} sec. That gives a power density of 10^{14} W/cm^2. If the energy reaches 400 MeV, the power density could be around 10^{16}-10^{17} W/cm^2. The most powerful picosecond lasers are in this power range. Energy loss processes, simulation of high current density beams, fluid dynamical pressures, surface target modifications, and interstellar collisions simulation will all be within the scope of studies with energetic clusters.

VI. LASER DESORPTION

It has already been demonstrated that very large biomolecules can be introduced in the gas phase by shooting with UV laser light on solid samples [70-72]. Molecules with masses larger than 100,000 were observed [72-78]. Very peculiar conditions have been established in the preparation of the samples, which, of course, are linked to emission processes.

For example, a dilute solution of the analyte (10^{-4}-10^{-5} mole/l) is mixed with a more concentrated solution of the matrix. A small amount of analyte/matrix is dried on a metallic sample holder (molar ratio $\simeq 10^{-4}$). Matrices as nicotinic acid or cinnamic acid have proved to be very useful and efficient. A very small amount of material is necessary (femtomole range). The method will certainly be very useful in the future and several laboratories are working on its development. Small and inexpensive UV lasers are now available, and analytical instruments can be easily built. Because of their ability to measure large masses, time of flight instruments are certainly very well adapted to matrix assisted laser desorption. An example of a TOF spectrum with masses up to 150,000 is shown in Fig. 26 from results obtained by the Rockefeller group [79].

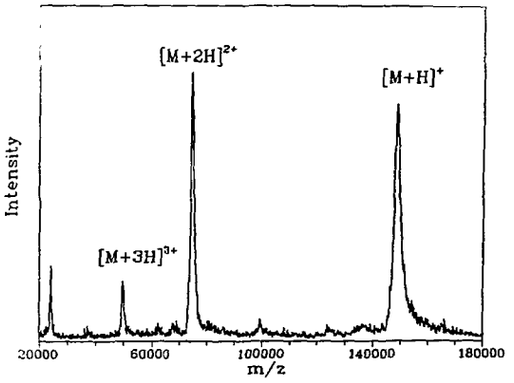

Figure 26
Mass spectrum of intact molecules ejected from a sample. Results from B.Chait and R.Beavis (Rockfeller University).

At Orsay, various TOF spectra have been obtained with the multidesorption probe TOF system TOF.23. A pulse N2 laser is used. An interesting spectrum (Fig. 27) recorded with TOF23 (IPN-Orsay) shows that molecular cluster ions of large molecules can be emitted by laser desorption. The number of molecules in the clusters depends on the mode of preparation of the sample and on the laser power. In Fig. 27 cluster ions of insulin molecules with m/z larger than 42000 are observed.

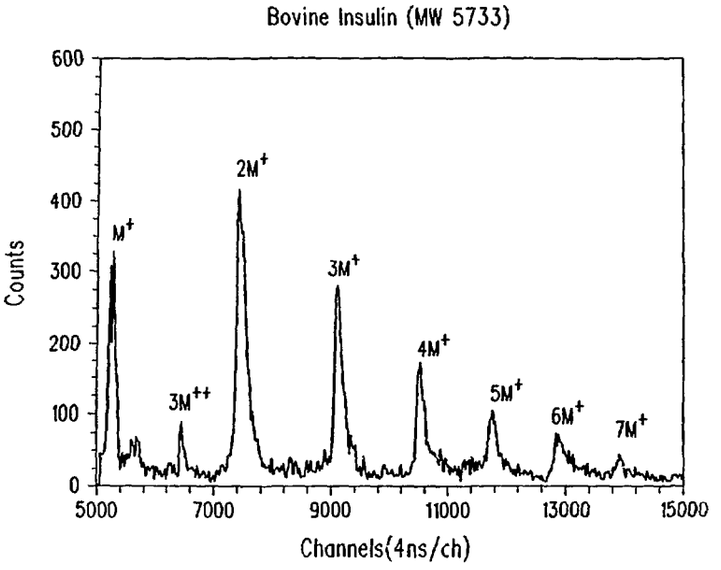

Figure 27
TOF mass spectrum of insulin cluster ions produced by matrix assisted laser desorption (Orsay)

In TOF spectra, a large number of low mass ions and neutrals are visible. They are formed at the surface of the sample (narrow peaks) and in the acceleration space (broad peaks). The rather broad mass region at apparent masses below 1000 is probably due to in-flight decompositions of matrix clusters in the acceleration region. The molecular ion peak shape of large molecules indicates that these ions are released from the surface of the solid sample at an early stage of the gas phase transition.

Intact molecular ions are emitted from the sample if the power density at the surface is small. This is defined by $P = W/S\tau$ where W is the energy per pulse, τ the duration of pulse, S the area of impact. It has been shown that a power density of around 10^6 watt/cm^2 can be considered as a desorption threshold value. The role of the matrix is very important since the laser wavelength must be strongly absorbed by the matrix molecules. Almost all of the energy is supposed to be absorbed in internal vibrations of the host molecules (matrix) and transfered to lattice vibrations on a time scale of 10^{-12} sec. The energy density in the lattice vibrations must increase very quickly to cause a "sublimation spike" producing an ejection of material containing the embedded large molecules into the gas phase. To be ejected, a substantial amount of momentum has to be transfered to the molecules.

Theoretical models [80,81] of matrix assisted laser desorptions try to explain the spectacular experimental results. As with keV and MeV ions these

models are certainly useful and can serve as a guide line to experimentalists who are still working to improve the method.

This recent discovery has opened new directions of research. Besides the theoretical aspects, the field of biology should benefit from the progress made to identify very large molecules. The detection of large molecular ions with small velocity is a crucial problem and efforts are being developed in several laboratories. Laser desorption experiments are rather simple to perform, and the equipment is now rather inexpensive. Time of flight techniques are mainly used.

The experimental results presented here, as well as new ideas to pursue this work in fundamental and applied physics and chemistry, are due to collective efforts from several people.

I would like to thank deeply my close collaborators S. DELLA-NEGRA, A. BRUNELLE, J. DEPAUW, C. DEPRUN. H. JORET has also been very much involved in this work. Collaborations with groups in France and other countries have been extremely fruitful and still contribute to the general dynamical processes of the development of the field.

I would like to acknowledge especially K. WIEN (Darmstadt), E. HILF (Oldenburg University), E.A. SCHWEIKERT (Texas A&M University), F. ROLLGEN (Bonn University), K.G. STANDING (Winnipeg University), I. BITENSKY (Elect. Inst. Tashkent), E. DA SILVEIRA (PUC Rio), G.B. BATISTA (PUC Rio) for their active participation in experiments or in discussions and interpretations.

I also thank G. BOLBACH (Inst. Curie, Paris), Y. HOPPILLIARD (Ecole Polytechnique, Palaiseau), P. SUDRAUD (Orsay Physics, Orsay), G. BEN ASSAYAG (CNET, Bagneux), G. MAYNARD and C. DEUTSCH (Orsay University).

This work would have not been done without the support of several good people at the laboratory, from the Electronic Workshop and Mechanical Workshop.

As usual, with the same efficiency and shrewdness, Evelyne D. has taken care of the manuscript and figures.

I do not forget my friend Douglas Barofsky (Oregon State University) who has kindly polished the english after, sometimes, long and interesting discussions on the physics and on the role of experimentalists !

The general support of IN2P3-CNRS is also greatly aknowledged.

Y. LE BEYEC

References

[1] Sigmund, P., Report Fysik Institut, Odense Univ. 1972, "Lectures on Collision Theory...", p. 3

[2] Wilson, W.D., Haggmark, L.G. and Biersack, J.P., Phys. Rev. B15, 2458 (1977).

[3] Ziegler, J.F., Biersack, J.P. and Littmark, H., "The stopping and ranges of ions in solids", vol. 1, Pergamon Press, New York (1985).

[4] Ritchie, R.H., Nucl. Instr. and Meth. 198, 1 (1982).

[5] Bethe, H.A., Ann. Phys. 5, 325 (1930).
Bethe, H.A., Z. Phys. 76, 293 (1932).

[6] Northcliffe, L.C., Schilling, R.F., Nucl. Data Table A7, 233 (1970).

[7] Ziegler, J.F. "The stopping and ranges of ions in matter", vol. 4, Pergamon Press, NY (1977).

[8] Hubert, F., Bimbot, R. and Gauvin H., Nucl. Data Tables, vol. 46, 1 (1990).

[9] Häkansson, P., Kamensky, I., Sundqvist, B., Nucl. Instr. and Meth. 198, 43 (1982) .

[10] Dück, P., Tren, W., Fröhlich, H. and Voit, H., Nucl. Instr. and Meth. 191, 245 (1981).

[11] Riggi, F., Nucl. Instr. and Meth. B43, 520 (1989).

[12] Della-Negra, S., Jacquet, D., Lorthiois, I., Le Beyec, Y., Becker, O., Wien, K., Int. J. of Mass Spectrometry and Ions Physics 53, 215 (1983).

[13] Salehpour, M. and Hunt, J.E., J. Phys. C2, 50, 155 (1989).

[14] Becker, O., Della-Negra, S., Le Beyec, Y. and Wien, K., Nucl. Instr. and Meth. B16, 321 (1986).

[15] Della-Negra, S., Le Beyec, Y., SIMS VI 1987, Edited by A.Benninghoven, H.Huber, H.W.Werner, J.Willey Sons (1988) p. 251

[16] Della-Negra, S., Depauw, J., Joret, H., Le Beyec, Y., J. Phys. C2, T50, 63 (1989).

[17] Le Beyec, Y., "Advances in Mass Spectrometry", vol. 11A (1989) 126, Ed. by P.Longevialle, Heyder and Son, London.

[18] Brown, W.L., Augustyniak, W.M., Lanzerotti, L.J., Johnson, R.E., Ewatt, R., Phys. Rev. Lett. 45, 1632 (1980).

[19] Bensenbacher, F., Bottiger, F., Graversen, O.,Hansen, J., Sorensen, H., Nucl. Instr. and Meth. 49, 203 (1980).

[20] Brown, W.L. and Johnson, R.E., Nucl. Instr. and Meth. B13, 295 (1986).

[21] Seiberling, L.E., Griffith, J.E. and Tombrello, T.A., Rad. Effects 52, 201 (1980).

[22] Voit, H., Nees, B., Niechler, E. and Frölich, H., Int. J. of Mass Spec trometry and Ions Physics 53, 201 (1983).

[23] Häkansson, P. and Sundqvist, B. Rad. Effects 69, 179 (1982).

[24] Della-Negra, S., Le Beyec, Y., Monard, B., Standing, K., Wien, K., Nucl. Instr. and Meth. B32, 360 (1988).

[25] Maynard, G. and Deutsch, C., Proc. of the First Workshop on Physics of Small Systems, Ed. by E.Hilf and K.Wien, Springer Series 269, 94 (1986).

[26] Baron, E. and Delaunay, B., Phys. Rev. A12, 40 (1975).

[27] Nikolaev, V.S. and Dmitriev, I.S., Phys. Lett. 28A, 277 (1968).

[28] Shima, K., Ishihara, T. and Mikumo, T., Nucl. Instr. and Meth. 200, 605 (1982).

[29] Bohr, N., Phys. Rev. 59, 270 (1941).

[30] Monart, B., Thesis, Université Paris Sud (1988).

[31] Wien, K., Becker, O., Guthier, W., Della-Negra, S., Le Beyec, Y., Monart, B., Standing, K., Maynard, G. and Deutsch, C., Int. J. of Mass Spectrometry and Ions Processes 78, 273 (1987).

[32] Danigel, I, Jungclas, H. and Schmidt, L., Int. J. of Mass Spectrometry and Ions Processes 52, 223 (1983).

[33] Bolbach, G., Della-Negra, S., Deprun, C., Le Beyec, Y., Rapid Communication in Mass Spectrom. 1, 22 (1987).

[34] Save, G., Häkansson, P., Sundqvist, B., Johnson, U., Soderstöms, E., Lindquist, E. and Berg, J., Appl. Phys. Lett. 51, 1379 (1987).

[35] Wien, K., Radiation Effects and Defects in Solids, 109, 137 (1987).

[36] Della-Negra, S., Depauw, J., Joret, H., Le Beyec, Y., Bitensky, I., Bolbach, G., Galera, M. and Wien, K., Nucl. Instr. and Meth. B52, 121 (1990).

[37] Sundqvist, B., this conference.

[38] Proc. of the Orsay Workshop, J. Phys. C2 (1989).

[39] Fenyo, D., Sundqvist, B.U.R. and Karlsson, B.R., Phys. Rev. B42, 1895 (1990).

[40] Della-Negra, S., Depauw, J., Joret, H., Le Beyec, Y., Schweikert, E.A., Phys. Rev. Lett. 6010, 948 (1988).

[41] Benguerba, I, Della-Negra, I, Joret, I, Le Beyec, I, Int. J. of Mass Spectrometry and Ions Processes (in press).

[42] Blain, M., Della-Negra, S., Park, M., Schweikert, E.A., unpublished results.

[43] Donets, E.D., Nucl. Instr. and Meth. B9, 532 (1985).

[44] Madey, T.E., Science 234, 316 (1986).

[45] Moshammer, R., Matthäus, R., Wien, K. and Bolbach, G., IFOS V, Edited by A.Hedin, B.Sundqvist and A.Benninghoven, J.Willey and Sons (1990), in press.

[46] Becker, O., Nucl. Instr. and Meth. 198, 53 (1982).

[47] Widdiyasekera, S., Hakansson, P., Sundqvist, B., Nucl. Instr. and Meth. B33, 836 (1988).

[48] Macfarlane, R., private communication and Jacobs, D.L., Ph.D. Thesis, Texas A&M University (1988).

[49] Fenyo, D., Thesis Uppsalla (1991) and to be published.

[50] Bitensky, I., Parilis, E., Della-Negra, S., Le Beyec, Y., to be published.

[51] Proc. of the workshop "Atomic Physics for Ion Driven Fusion IV", Edited by C.Deutsch, J. Phys. C7 (1988).

[52] Betz, H. and Grodzins, L., Phys. Rev. Lett. 25, 211 (1970).
Betz, H., Nucl. Instr. and Meth. 132, 19 (1976).

[53] Brunelle, A., Della-Negra, S., Depauw, J., Joret, H., Le Beyec, Y., Wien, K., Nucl. Instr. and Meth. B43, 484 (1989).

[54] Betz, H.D., Rev. Mod. Phys. 44, 465 (1972).

[55] Bohr, N. and Lindhard, J., Mat. Fys. Medd. Danske Vid. Selsk 26, 7 (1954).

[56] Benninghoven, A., Org. Mass Spectrom. 12, 595 (1977).

[57] Andersen, H.H. and Bay, H.L., J. Appl. Phys. 46, 246 (1975).

[58] Thompson, D.A., Hohar, S.S., Appl. Phys. Lett. 34, 342 (1979).

[59] Reuter, W., Anal. Chem. 59, 2081 (1988).

[60] Zalm, P.C. and Becker, L.J., J. Appl. Phys. 56, 220 (1984).

[61] Beuhler, J. and Friedman, L., Chem. Rev. 86, 521 (1986).

[62] Thomas, J.P., Filpus-Luyckx, D.E., Fallavier, M., Schweikert, E.A., Phys. Rev. Lett. 55, 1, 103 (1985).

[63] Kamensky, I., Häkansson, P., Sundqvist, B., McNeal, C. and Macfarlane, R., Nucl. Instr. and Meth. 198, 65 (1982).

[64] Blain, M.G., Schweikert, E.A. and da Silveira, E.F., J. Phys. 50, C2, 85 (1989).

[65] Blain, M.C., Della-Negra, S., Joret, H., Le Beyec, Y. and Schweikert, E.A., Phys. Rev. Lett. 63, 15, 1625 (1989).

[66] Sudraud, P. and Ben Assayag, G., Orsay Physics Company, Orsay.

[67] Brunelle, A., Thesis Orsay Paris Sud (1990).

[68] Benguerba, M., Brunelle, A., Della-Negra, S., Depauw, J., Joret, H., Le Beyec, Y., Blain, M.G., Schweikert, E.A., Ben Assayag, G., Sudraud, P., IPNO-DRE-91-16.

[69] Della-Negra, S., Gardès, D., Le Beyec, Y., Projet ORION, IPN Orsay (1990).

[70] Tanaka, K., Waki, H., Ido, Y., Akita, S., Yoshida, Y. and Yoshida, Y., Rapid Communication in Mass Spectrom. 2, 151 (1988).

[71] Karas, M. and Hillenkamp, F., Anal. Chem. 60, 2299 (1988).

[72] Karas, M., Bohr, U. and Hillenkamp, F., Int. J. of Mass Spectrometry and Ions Processes 92, 231 (1989).

[73] Salehpour, M., Perera, I., Kjellberg, J., Hedin, A., Islamian, M.A., Hakansson, P. and Sundqvist, B.U.R., Rapid Communication in Mass Spectrom. 3, 259 (1989)

[74] Nelson, R.W., Rainbow, M.J., Lohr, D.E. and Williams, P., Science 246, 1585 (1989).

[75] Karas, M., Bahr, U., Ingendoh, A. and Hillenkamp, F., Angew. Chem. (Int. Ed., Engl) 28, 760 (1989).

[76] Beavis, R.C. and Chait, T., Rapid Communication in Mass Spectrom. 3, 233 (1989).

[77] Beavis, R.C. and Chait, T., Rapid Communication in Mass Spectrom. 3, 432 (1989).

[78] Beavis, R.C. and Chait, T., Rapid Communication in Mass Spectrom. 3, 432 (1989).

[79] Beavis, R. and Chait, B., Proc. of the 38th ASMS Conference (1990) p. 26.

[80] Vertès, A., Gigbels, R., Levine, R.D., Rapid Communication in Mass Spectrom. 4, 6 (1990).

[81] Johnson, R.E., Banergee, S., Hedin, A., Fenyo, D. and Sundqvist, B.U.R., Proc. of the "Minaki Meeting on Large Molecules", Canada (1990), in press.